Dynamics of Barrier Crossing in Classical Nucleation Theory†

Robert McGraw

Atmospheric Sciences Division, Environmental Sciences Department, Brookhaven National Laboratory, Upton, New York 11973

Received: May 18, 2001; In Final Form: July 13, 2001

The dynamics of nucleation barrier crossing is examined using Becker−Doring kinetics, matrix methods, and stochastic model simulation. Fundamental connections between resistance to crossing and fluctuations in cluster size are derived using the Kubo−Nyquist relations. For analysis of nucleation kinetics, the matrix approach of Shugard and Reiss is supplemented with a novel extension based on recursion/projection operator methods. The combined approach yields nested sequences of upper and lower bounds to the relaxation rates of clusters coupled to a thermal bath. Fluctuations are studied using simulations based on a stochastic model of cluster evaporation/growth. Under typical conditions, it is found that relaxation from the top of the barrier is slow, due to multiple re-crossings, and the transmission coefficient for nucleation is small and extremely difficult to estimate from single-cluster simulations using standard Bennett−Chandler and Kramers models. A new approach based on relaxation on a "dual" potential surface is introduced. It is shown that the dual model provides an optimal weighted cluster sampling and reliable estimation of the transmission coefficient (to within a few percent). Collectively, these methods address the efficient determination of nucleation rates from computer simulations of individual cluster evaporation/growth events.

1. Introduction

In their simulation capacity, and with a consistent cluster definition, computers provide a unique source of statistical information on the molecular addition/loss steps that are responsible at equilibrium for fluctuating changes in cluster size.[1−4] Simulations can lead to reliable estimates of cluster energy,[1] although care must be taken that the translational energy is properly included.[5] Fluctuations in cluster energy, and statistical information about the frequencies of condensation and evaporation events and changes in cluster size and shape are also valuable products of simulation the lie beyond the scope of phenomenological nucleation models. Here, two issues arise: The first derives from the fact that the height of the nucleation barrier is typically much larger than kT. As a result, those clusters that most control the kinetics of nucleation are exceedingly rare and difficult to sample using conventional Boltzmann statistics. This necessitates sampling with respect to unconventional ensembles, tailored to compensate for the fact that the frequency of appearance of clusters in the critical size range is exceedingly small. For example, the nucleation barrier has been obtain in a molecular simulation study using umbrella sampling methods,[1] and the recent development of iterative multicanonical methods, applied to similar problems of first-order phase transformation, should also be noted.[6] In these approaches, external potentials, which are a priori unknown and have to be determined, are applied to constrain the dynamics to selected regions of phase space over which statistical sampling takes place. An optimized weighting potential for sampling clusters in the critical-size range most important to nucleation is presented in section 5.

The second issue facing molecular simulations is the ability to represent only one cluster, or at most several clusters, in the simulation volume at any one time. Thus, one is faced with determining nucleation kinetics from the simulated dynamics of individual clusters exchanging molecules with their (supersaturated) environment. The problem is exacerbated by the fact that although typical nucleation barrier heights greatly exceed kT, the barriers themselves tend to be flat in the sense that many different size clusters will typically have energies within kT of the barrier height. As a result, diffusive recrossings of the barrier are the rule and the methods of transition state theory, which assume no recrossing, are difficult to apply. Although some progress has been made in extending the Bennett−Chandler scheme to diffusive barrier crossing,[2,7] a Kramers picture,[8] which has been shown to be more general in the sense that the reactive flux (Bennett−Chandler) method is recovered in the high barrier limit,[9] may be a more natural description. The present examination of barrier crossing using Becker−Doring kinetics (section 2) suggests that this "high barrier limit" is much too high to support any significant nucleation rate. For this reason, we adopt the Kramers description in the present study, but even here the problem of determing nucleation rates from the simulated dynamics of individual clusters remains difficult and new approaches, perhaps along the lines suggested toward the end of this paper, are required.

In section 2, we review the dynamics of barrier crossing within the framework of the Becker−Doring multistate kinetics model. The only assumptions required are validity of detailed balance and rapid equilibration of clusters to the temperature of their surroundings on the scale of the average time between cluster evaporation/growth events. Validity of detailed balance is supported by recent molecular dynamics simulations of cluster size during the equilibration of a single cluster in a small container volume.[3] Here, good agreement was found when the transitions $g \rightarrow g + 1$ and $g + 1 \rightarrow g$ were enumerated and compared with the detailed balance prediction over the range of cluster sizes, g, included in the simulation. The barrier transmission coefficient, which is inversely correlated with the number of recrossings, is shown in section 2 to be small due to the typically large number of mutually accessible clusters near

† Part of the special issue "Howard Reiss Festschrift".

10.1021/jp011914q CCC: $20.00
Published on Web 09/15/2001

the top of the barrier, which are strongly coupled to each other through molecular exchange with the surrounding bath. In the Kramers picture, this strong coupling is characteristic of a highly diffusive regime in which further increases in coupling lower the barrier transmission rate.[8]

The dynamics of cluster relaxation is examined in section 3 using a new matrix-recursion method. Addition of the recursion method supplements the matrix approach to nucleation kinetics developed by Shugard and Reiss.[10] The matrix approach, on its own, provides a powerful and complete description of the global Becker−Doring model; yielding transient kinetics as well as steady-state nucleation rate. Its supplementation with the recursion method allows one to obtain a local description of the kinetics, which is ideal for studying the dynamics of individual clusters. By focusing on clusters of near critical size, recursion enables one to project out the most important degrees of freedom governing the kinetics of the global nucleation process. Additionally, the method provides nested pairs of upper and lower bounds to the cluster relaxation rate. In section 5, this relaxation is linked to the barrier transmission coefficient and nucleation rate.

The matrix-recursion method provides information on the continuous evolution of the probability that clusters are of a specific size. Fluctuations and noise are treated using Kubo and Nyquist methods[11,12] in section 4. The fluctuations in cluster size are correlated with the resistance to single-cluster motion along the coordinate of cluster size using the Nyquist relation. This section presents a Nernst−Planck description for the total nucleation flux and an equivalent Langevin description for the Brownian-like motion of clusters in size space. It is suggested that a fruitful analysis can be made of the random current fluctuations in the Langevin equation leading ultimately to a statistical estimation of the key transport parameters in terms of which the nucleation rate can be obtained. In essence, the nucleation process is treated as a Brownian walk in a potential consisting of the nucleation barrier itself. These ideas, which can be found in related forms in the literature,[13−15] are made explicit in section 4 through the introduction of a shot noise model for fluctuations during cluster evaporation and growth, which is also the basis for the stochastic model simulations of section 5.

Results from multiple simulation runs are averaged and compared with nested bounds on the relaxation rate obtained by the matrix-recursion method in section 5. This section also presents calculations for a dual potential surface obtained by reversing the sign of the barrier force. Dualities between relaxation to equilibrium for the dual (well-shaped) potential and relaxation to a nonequilibrium steady state of constant nucleation rate for the barrier are described. The dual well potential is shown to provide the optimal weights for determining barrier transmission coefficients and nucleation rates through non-Boltzmann sampling. Finally, the idea of applying real-space renormalization techniques[16] to obtain a different kind of reduce-dimensionality description of the nucleation kinetics is briefly discussed. The present focus on classical nucleation theory, for which the detailed kinetics is known a priori, provides a testing ground for the analytic methods and may well provide a qualitative guide to the dynamics of barrier crossing for more fundamental molecular models of nucleation as these are developed.

2. Background

This section begins with a brief review of the Becker−Doring kinetics scheme in order to establish the model framework and notation for what follows. For a more complete description see ref 17. A substance-independent calculation of the barrier transmission coefficient, as a function of critical cluster size and energy, is also presented below within the framework of Becker−Doring kinetics.

2.1 Becker−Doring Kinetics. The net flux for conversion of clusters of size g to size $g + 1$ is

$$J_{g,g+1} = \beta_g f_g - \gamma_{g+1} f_{g+1} \tag{2.1}$$

where f_g is the actual number density of g-mer clusters and β_g-(γ_g) is the rate at which single molecules are added to (lost from) the g-cluster. At equilibrium, according to detailed balance, the net currents vanish to give

$$\beta_g n_g - \gamma_{g+1} n_{g+1} = 0 \tag{2.2}$$

Here, n_g is the constrained equilibrium concentration of g-clusters. The constrained equilibrium concentration of monomer, n_1, is related to n_g and n_{g+1} through the reversible chemistry $A_g + A_1 \leftrightarrow A_{g+1}$ according to the law of mass action

$$K_g^{\mathrm{eq}}(T) = \frac{[A_{g+1}]}{[A_1][A_g]} \cong \frac{n_{g+1}}{n_g n_1} \tag{2.3}$$

where A_g denotes a cluster containing g monomers, $[A_g]$ is the activity of these clusters, and $K_g^{\mathrm{eq}}(T)$ is a function of temperature alone. The last equality, the law of mass action, applies to an ideal mixture of clusters for which activity is proportional to number concentration. The population ratio appearing in eq 2.3 is given by the Boltzmann distribution

$$\frac{n_{g+1}}{n_g} = \frac{\beta_g}{\gamma_{g+1}} = \exp\{-[W(g+1) - W(g)]/kT\} \tag{2.4}$$

where the first equality is from eq 2.2 and $W(g)$ is the reversible work of forming a cluster of size g.

Using eq 2.2 to eliminate the evaporation rate, eq 2.1 becomes

$$J_{g,g+1} = \beta_g n_g \left(\frac{f_g}{n_g} - \frac{f_{g+1}}{n_{g+1}} \right) \tag{2.5}$$

At steady-state, the current is constant ($J_{g,g+1} = J$), independent of g, and eqs 2.5 may be summed to give the Becker−Doring nucleation rate

$$J = \left(\frac{f_1}{n_1} - \frac{f_G}{n_G} \right) \left(\sum_g \frac{1}{\beta_g n_g} \right)^{-1} = \left(\sum_g \frac{1}{\beta_g n_g} \right)^{-1} \tag{2.6}$$

In obtaining the last equality, the Szilard and monomer boundary conditions, $f_G = 0$ and $f_1/n_1 = 1$, respectively, where G is set significantly larger (e.g., twice) the critical cluster size, were used. The insensitivity of J to the precise location of these boundaries is discussed below.

2.2 Barrier Transmission Coefficient. Ordinary transition state theory does not account for barrier recrossing once the critical nucleus is formed and J, at this level of approximation, is simply the product of the number of molecules at the top of the barrier (assuming equilibrium with the reactant) and crossing rate[2]

$$J_{\mathrm{TST}} = \beta_{g^*} n_{g^*} \tag{2.7}$$

The correction factor required to recover the true current is the barrier transmission coefficient, κ- also known in nucleation

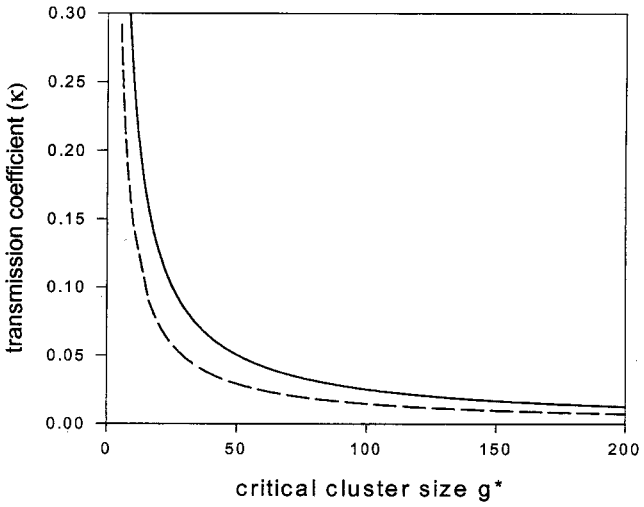

Figure 1. Barrier transmission coefficient (κ) as a function of critical cluster size according to classical nucleation theory. Results are shown for nondimensional barrier heights of $W^*/kT = 60$ (solid) and $W^*/kT = 20$ (dashed) curves.

theory as the Zeldovich factor[17]

$$J = \kappa J_{\mathrm{TST}} = \kappa \beta_{g^*} n_{g^*} \tag{2.8}$$

For Becker−Doring kinetics, the precise value of κ is available from eqs 2.6 and 2.7

$$\kappa = \left(\sum_g \frac{\beta_{g^*}}{\beta_g}\frac{n_{g^*}}{n_g}\right)^{-1} \cong \left(\sum_g \frac{n_{g^*}}{n_g}\right)^{-1} \tag{2.9}$$

The last equality neglects dependence of the monomer addition rate on surface area by setting $\beta_g = \beta_{g^*}$. This is generally an excellent approximation (see below) that will be used again in section 5. For generality, the g dependence of β_g will otherwise be retained.

To be quantitative for a specific cluster model, we turn to an evaluation of κ with $W(g)$ from the capillarity approximation of classical nucleation theory (CNT). Results will be kept in sufficiently general form as to have relevance, like CNT itself, to both vapor and condensed phase, homogeneous or heterogeneous, nucleation processes. The CNT barrier assumes the form

$$W_{CNT}(g) = -g\Delta\mu + \alpha g^{2/3} = -2W^*\left(\frac{g}{g^*}\right) + 3W^*\left(\frac{g}{g^*}\right)^{2/3} \tag{2.10}$$

consisting of bulk and surface terms proportional to g and $g^{2/3}$, respectively. The coefficient α includes surface tension and nucleus shape (both assumed independent of g) and $\Delta\mu$ is the bulk free-energy difference driving the phase change. The two parameters, $\Delta\mu$ and α determine the critical size, g^*, where $W_{CNT}(g)$ assumes its maximum value, and the barrier height $W^* = W_{CNT}(g^*)$. In the last equality of eq 2.10, $W_{CNT}(g)$ has been expressed in terms of g^* and W^*, showing that all nucleation barriers have the same overall shape in CNT, independent of substance. Accordingly, different substances will have the same cluster ratios n_{g^*}/n_g and same barrier transmission coefficient (according to the approximate equality of eq 2.9) when compared at the same values of g^* and W^*.

Figures 1 and 2 show general features of the barrier transmission coefficient (κ) in CNT. Figure 1 shows κ as a function of critical size for $W^* = 60kT$ (solid curve) and $W^* = 20kT$(dashed curve). These are typical barrier heights for homogeneous and heterogeneous nucleation processes, respectively.[18] It follows from eqs 2.4, 2.9, and 2.10 that these curves, which for $g^* \geq 5-10$ vary inversely with g^*, are substance-independent. It is worth noting here for later use that the results obtained by the approximate equality of eq 2.9 are indistinguishable from those shown in the figure. For example, for $W^* = 60\ kT$ and $g^* = 100$, $\kappa = 0.02517$ for the equality and 0.02524 for the approximate equality. Finally, one sees from Figure 1 that κ increases slightly with barrier height. However, for this coefficient to approach unity, thus validating application of transition state theory, the barrier would have to be insurmountably high—well beyond the range of interest to nucleation theory.

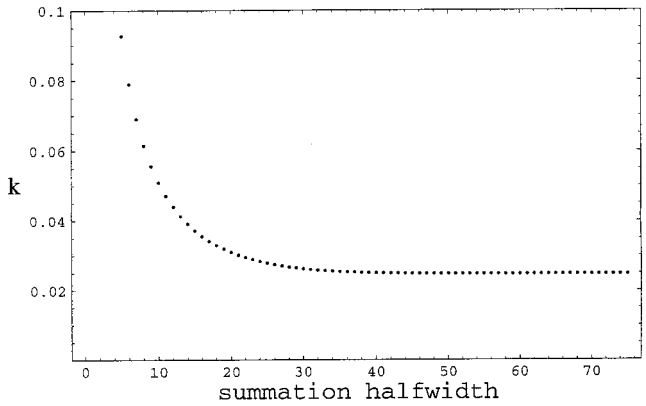

Figure 2. Sequence of approximations to (κ) generated by including increasing numbers of near-critical clusters in the summation of eq 2.9. The included clusters are $g = g^*$, $g^* \pm 1$, $g^* \pm 2$, ..., $g^* \pm m$ where m is the summation half-width.

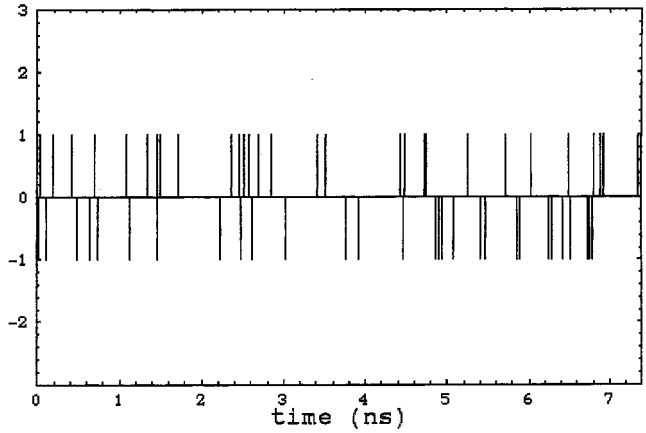

Figure 3. Sampled sequence of cluster evaporation and growth events from the stochastic model. The collision rate is that for vapor−liquid nucleation of water and a near critical cluster under conditions for which $g^* = 100$. Under these conditions, the average time between growth events is $(\beta_{g^*})^{-1} \cong 2.47 \times 10^{-10}$ sec. Depicted here are the delta function currents for growth, $J^+(t)$, and for evaporation, $J^-(t)$, as bars of height equal to plus and minus unity, respectively. The gain/loss of higher-order clusters is neglected.

Equations 2.6 and 2.9 show clearly that the most important contributions to J and to κ are from clusters near critical size, where n_g assumes its minimum value. Figure 2 shows the result of a series of approximations to κ generated by summing over all terms of eq 2.9 for which the summation index equals g^*, $g^* \pm 1$, $g^* \pm 2$, ..., $g^* \pm m$ as a function of the summation half-width m. Here, it is seen that not just the critical cluster, but a large number of clusters on either side of g^*, here about 40 ($m \cong 20$) contribute significantly to κ and therefore to nucleation rate. On the other hand, beyond this range there is

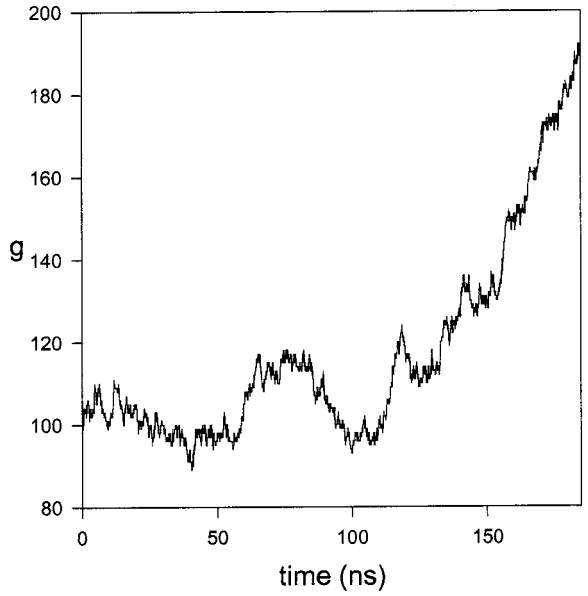

Figure 4. Cluster size as a function of time. Conditions are the same as in Figure 3. The figure shows excursions about the critical size followed at later time by sustained growth beyond the barrier. In other cases, which occur with about equal frequency, evaporation of the cluster occurs. This sample trajectory shows both the slowness of the relaxation from critical size and the multiple barrier recrossings.

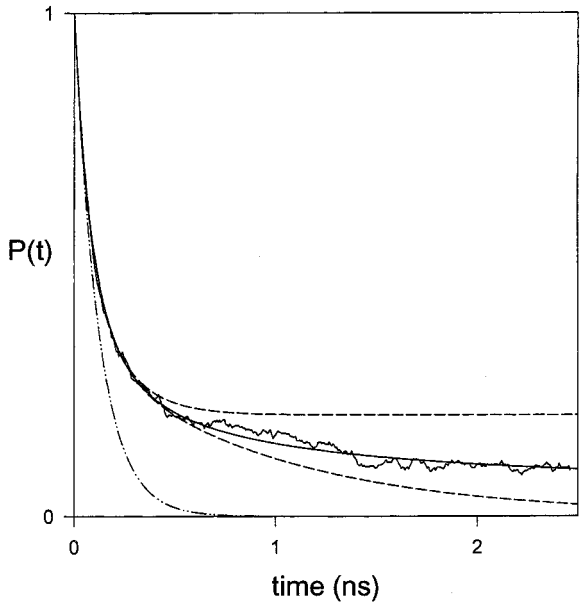

Figure 5. Bounds on the relaxation of a critical cluster and comparison with the stochastic model. Conditions are the same as in Figures 3 and 4. Shown are the lower bound for $k = 1$ (dashed-dotted curve), the third ($k = 3$) upper and lower bound pair (dashed curves), the tenth ($k = 10$) upper and lower bounds (smooth curves converged on the scale of the figure). Also shown is the simulated decay from the stochastic model averaged over 1000 runs (noisy solid curve).

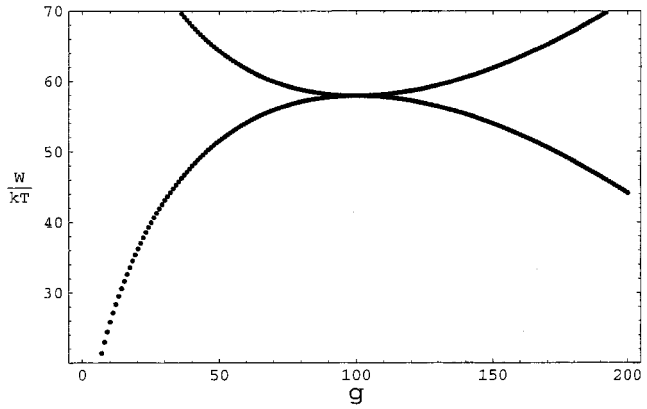

Figure 6. Nucleation barrier and dual well for the nucleation of water vapor under the conditions of Figures 3−5.

little contribution demonstrating, the insensitivity of J to placement of the equilibrium and Szilard boundary conditions; both boundaries could have been moved much closer in toward g^* without significantly changing the predicted nucleation rate.

The results of this section demonstrate that small values of κ are inherent in classical nucleation theory. This is due to the general feature that the nucleation barrier tends to be flat near g^* to the extent that many clusters typically lie within only a few kT of the barrier height, and these are the clusters that contribute to κ and to J. (See, for example, the lower curve in Figure 6, which shows the classical barrier for $g^* = 100$ and W^* near 60 kT.) From eq 2.10, the number of clusters within kT of the barrier height is proportional to g^*. For $g^* = 100$, about 40 clusters are within kT of W^*—an ample illustration of mutual accessibility of near critical clusters due to barrier flatness on the scale of monomeric changes in cluster size! Accordingly, during a cluster growth sequence, multiple recrossings of the barrier are likely to occur and this, in turn, implies a barrier transmission coefficient much less than unity. These expectations are borne out by the analytic techniques described below and by the stochastic model simulations of Sec 5.

3. Dynamics of Relaxation from the Top of the Free-Energy Barrier

The relaxation properties of a critical nucleus are determined in this section by the matrix-recursion method, which is developed here and applied to the master equations governing multistate nucleation kinetics. The "matrix" part of the matrix-recursion method consists of the general theoretical framework developed by Shugard and Reiss.[10] Molecular rate constants are determined from detailed balance considerations and used in the construction of a Hermitian matrix (**H**) whose eigenvectors and eigenvalues carry the overall rate information. This matrix formulation of nucleation kinetics forms the basis (in section 3.2) for extension of the recursion method[19] to nucleation. The matrix-recursion method is applied here to describe the averaged relaxation of clusters from the top of the free-energy nucleation barrier. It provides a systematic procedure for abstracting, from the full kinetic information contained in **H**, the most relevant (nested) subspaces for describing the nucleation dynamics. Here, an extended form of the recursion method, originally developed to model excitation transfer in disordered media,[20] and having the property of yielding nested sequences of upper and lower bounds to the full dynamics with increasing subspace dimension is adapted. A simpler and much more direct motivation of the recursion is presented here using moment and quadrature methods recently developed as part of a new approach to aerosol dynamics simulation.[21,22]

3.1 Matrix Formulation of Shugard and Reiss. Evolution of the cluster population, f_g, is given in terms of nucleation currents

$$\frac{\mathrm{d}f_g}{\mathrm{d}t} = J_{g-1,g} - J_{g,g+1} \tag{3.1}$$

Substitution from eq 2.5 gives the following set of master

equations

$$\frac{df_g}{dt} = \beta_{g-1} f_{g-1} - \left(\beta_g + \beta_{g-1}\frac{n_{g-1}}{n_g}\right) f_g + \beta_g \frac{n_g}{n_{g+1}} f_{g+1} \qquad (3.2)$$

Depending on the problem of interest, one applies the appropriate boundary conditions to eqs 3.2 to terminate the sequence. For example, if the steady-state nucleation current is desired, a constant source term for monomer is included[10] and the sequence of kinetic equations extends from $g = 2$ to $g = G - 1$. Here, we are interested in transient solutions for which a convenient vector-matrix form of eqs 3.2 is appropriate[10]

$$\frac{d\mathbf{f}}{dt} = \mathbf{K}\mathbf{f} \qquad (3.3)$$

The components of the column vector **f**, whose dimension remains for now unspecified, are the cluster populations, f_g. Elements of **K** follow inspection of eqs 3.2

$$K_{g,g-1} = \beta_{g-1}$$

$$K_{g,g} = -\beta_g - \beta_{g-1}(n_{g-1}/n_g)$$

$$K_{g,g+1} = \beta_g(n_g/n_{g+1})$$

Although **K** is nonsymmetric, its off-diagonal elements are related through the detailed balance condition. Rewriting the nucleation current, $J_{g,+1}$, from eq 2.5 gives

$$J_{g,g+1} = K_{g+1,g} f_g - K_{g,g+1} f_{g+1} \qquad (3.4)$$

Under the conditions of constrained equilibrium, $J_{g,g+1} = 0$ and

$$K_{g+1,g} = K_{g,g+1}(n_{g+1}/n_g) = K_{g,g+1}\exp\{[W(g) - W(g+1)]/kT\} \qquad (3.5)$$

As shown in ref 10, detailed balance provides the basis for converting **K** to Hermitian form. Introducing the diagonal matrix, **D**, with elements

$$D_{g,g} = \exp[W(g)/kT] \qquad (3.6)$$

enables the detailed balance condition (eq 3.5) to be expressed as

$$\mathbf{K^T} = \mathbf{DKD^{-1}} \qquad (3.7)$$

where $\mathbf{K^T}$ is the transpose of **K**. Finally, consider the matrix **H** defined as

$$\mathbf{H} = -\mathbf{D^{1/2}KD^{-1/2}} \qquad (3.8)$$

where $\mathbf{D^{1/2}}$ is the square root of **D**. Then

$$\mathbf{H^T} = -(\mathbf{D^{1/2}KD^{-1/2}})^{\mathbf{T}} = -\mathbf{D^{-1/2}K^TD^{1/2}} = -\mathbf{D^{-1/2}DKD^{-1}D^{1/2}} = -\mathbf{D^{1/2}KD^{-1/2}} = \mathbf{H}$$

where the third equality follows from detailed balance (eq 3.7). This shows that **H** is Hermitian. From eq 3.8, its elements are

$$H_{i,j} = -D_{i,i}^{1/2} K_{i,j} D_{j,j}^{-1/2} \qquad (3.9)$$

In the frame of the transformed matrix **H**, eq 3.3 becomes

$$\frac{d\psi}{dt} = -\mathbf{H}\psi \qquad (3.10)$$

where

$$\psi = \mathbf{D^{1/2}f} \qquad (3.11)$$

The formal solution to eq 3.10 is

$$\psi(t) = \exp(-\mathbf{H}t)\psi(0) = \mathbf{V}\exp(-\mathbf{D}_\lambda t)\mathbf{V^{-1}}\psi(0) \qquad (3.12)$$

where **V** diagonalizes **H**

$$\mathbf{V^{-1}HV} = \mathbf{D}_\lambda \qquad (3.13)$$

$\mathbf{D}_\lambda$, not to be confused with the transformation matrix **D** of eq 3.6, is the diagonal matrix having the eigenvalues of **H** as elements

$$(\mathbf{D}_\lambda)_{ii} = \lambda_i \qquad (3.14)$$

and the columns of **V** consist of the corresponding eigenvectors, $\mathbf{V}_i$, of **H**. With these definitions, eq 3.12 can be put into a more explicit form. In Dirac notation

$$|\psi(t)\rangle = \sum_i \langle \mathbf{V}_i|\psi(0)\rangle \exp(-\lambda_i t)|\mathbf{V}_i\rangle \qquad (3.15)$$

showing the full time-dependent solution in terms of the eigenvalues and eigenvectors of **H**. For single-component nucleation the dimensionality of **H** is order G, which may only be a few hundred molecules. For binary nucleation, on the other hand, the dimensionality of **H** can easily exceed several thousand. Nevertheless, because **H** is banded and sparse (**H** is tridiagonal for the 1D kinetics considered here), efficient numerical methods are available, and the matrix method has been used to provide a complete 2D network description of binary nucleation kinetics.[23] These considerations set the stage for application of the recursion method.

3.2 Application of the Recursion Method. The recursion method provides a powerful technique for simulation of "local" dynamical processes in extended strongly interacting systems. Thus, although 3.15 furnishes a full global description of the nucleation kinetics, the fact that the clusters contributing with greatest weight to the nucleation rate are those near to the critical size suggests that the full dynamics contains more information then required and that the problem can be substantially reduced using a local kinetics approach. The recursion method is ideal for tracking the local dynamics of averaged single cluster motion from a specified initial condition and will now be applied to the relaxation of clusters undergoing molecular exchange with a supersaturated parent phase.

Consider a single cluster exchanging molecules with a surrounding bath at fixed temperature and chemical potential. As the initial condition, we set the probability that the cluster is of size g^* at $t = 0$ to unity. Accordingly, the normalized ket $|\psi(0)\rangle$ consists of a column vector of zeros with unity at the

position corresponding to g^*

$$|\psi(0)\rangle = |g^*\rangle = \begin{pmatrix} 0 \\ \cdot \\ \cdot \\ 1 \\ \cdot \\ 0 \end{pmatrix} \tag{3.16}$$

The probability that the cluster has g^* molecules at time t is given by the projection

$$P(t) \equiv \langle\psi(0)|\psi(t)\rangle = \sum_i |\langle V_i|\psi(0)\rangle|^2 \exp(-\lambda_i t) = \int_0^\infty N_0(\lambda) \exp(-\lambda t) d\lambda \tag{3.17}$$

where eq 3.15 has been used. The last equality shows that the time-dependent projection of $|\psi(t)\rangle$ onto the initial condition is given by the Laplace transform of the local density of states distribution defined as[19]

$$N_0(\lambda) = \sum_i |\langle V_i|\psi(0)\rangle|^2 \delta(\lambda - \lambda_i) \tag{3.18}$$

The right side of eq 3.18 is a sum of weighted delta functions centered on the eigenvalues of **H**.

The extended recursion method[20] provides an algorithm for generating nested sequences of upper and lower bounds to $P(t)$ without having to solve the full eigensystem required by eq 3.17; only the lower-order moments of $N_0(\lambda)$ are required. To describe the algorithm, we begin by noting that multiplication of $|g^*\rangle$ by **H** produces a new vector, $\mathbf{H}|g^*\rangle$, which includes probability for occupation of the nearest neighboring sizes of g^*, as well as g^* itself. Multiplication again by **H** introduces occupation probability for the next nearest sizes, etc. The essence of the recursion method lies in its property of tracking of the dynamics in the k-dimensional subspace spanned by the Krylov vector sequence generated in this manner

$$\{|\psi(0)\rangle, \mathbf{H}|\psi(0)\rangle, \mathbf{H}^2|\psi(0)\rangle, ..., \mathbf{H}^{k-1}|\psi(0)\rangle\} \tag{3.19}$$

In this Krylov vector space we define the moments of $N_0(\lambda)$

$$\mu_l = \langle\psi(0)|\mathbf{H}^l|\psi(0)\rangle = \int_0^\infty \lambda^l N_0(\lambda) d\lambda \tag{3.20}$$

The last equality follows in a fashion similar to showing that $P(t)$ is the Laplace transform of $N_0(\lambda)$.

A key feature of the extended recursion method is that bounds on $P(t)$ can be obtained directly from the moments. The previous derivation of this result,[20] which was based on a product-difference algorithm due to Gordon,[24] is simplified here by exploiting well-known connections between moments and quadrature methods.[21,22] The algorithm proceeds in two steps. In the first, the first $2k-1$ integral moments are used to generate the following tridiagonal Jacobi matrix

$$\mathbf{T}_k = \begin{pmatrix} a_1 & b_1 & & \\ b_1 & a_2 & \cdot & \\ & \cdot & \cdot & b_{k-1} \\ & & b_{k-1} & a_k \end{pmatrix} \tag{3.21}$$

In general $\mathbf{T}_k$ will have dimensionality considerably smaller than **H**. There are a number of interconnected approaches, under the general heading of moment methods, for generating the elements of $\mathbf{T}_k$ from the first $2k-1$ integral moments. These include Lanczos tridiagonalization,[19] a product-difference algorithm used to obtain related bounds on the partition function by Gordon,[20,24] and projection operator methods for generating continued fraction solutions to the generalized Langevin equation.[25] A compact algorithm is available in the subroutine ORTHOG from Numerical Recipes.[26] Our experience with aerosol moments[22] supports ORTHOG as a highly efficient and robust approach to generating $\mathbf{T}_k$ from moments. Nevertheless, inverting integral moments of high order is known to be ill-conditioned,[26] and we find that it is best to limit the dimensionality (k) of $\mathbf{T}_k$ to about 20.

Solution of the eigenvalue problem associated with $\mathbf{T}_k$ yields quadrature abscissas and weights,[21] which in turn furnish a sequence of nondecreasing lower bounds to $P(t)$ for increasing k.[20] These solutions are in the form of k-point quadrature approximations to the integral of eq 3.17

$$P_{\mathrm{LB}(k)}(t) = \sum_{i=1}^{k} |\langle V_i^{LB}|\psi(0)\rangle|^2 \exp(-\eta_i^{LB} t) \tag{3.22}$$

where $\{\eta_i^{LB}\}$ are the eigenvalues, and $\{\mathbf{V}_i^{LB}\}$ the corresponding eigenvectors, of $\mathbf{T}_k$.

A physical understanding of connection between $\mathbf{T}_k$ and **H** is had by observing that eq 3.21 represents a partial similarity transformation of **H**. Letting Q_i denote occupation of the i^{th} transformed basis site, the transformed kinetic equations are

$$\frac{dQ_1}{dt} = -a_1 Q_1(t) + b_1 Q_2(t)$$

$$\frac{dQ_2}{dt} = b_1 Q_1(t) - a_2 Q_2(t) + b_2 Q_3(t)$$

$$\frac{dQ_k}{dt} = b_{k-1} Q_{kn-1}(t) - a_k Q_k(t) \tag{3.23}$$

The secular equation in the new (Lanczos) basis, derived from the moments is, thus, tridiagonal and the partial transformation can be viewed as generating a set of k equivalent "sites" with connectivity of a linear chain and nearest neighbor couplings. (This 1D nearest neighbor coupling in the Lanczos basis is independent of spatial dimensionality and degree of coupling in the original basis, which just happens to be nearest neighbor and 1D for the case of single component clusters and monomer exchange considered here.) The initial condition on eqs 3.23 is given by having unit excitation on the first chain site, $Q_1(0) = 1$, and zero elsewhere. The rates of transfer to the rest of the chain convey the dynamics in the transformed basis, from which the dynamics in the original basis is readily determined. Exploiting the 1D connectivity of the chain, we can give a simple geometric interpretation to the existence of nested bounds on $P(t)$: Truncation of the transformed kinetic equations at level k, as in eqs 3.23, results in a lower bound to the true relaxation $P(t)$. This is apparent from the equations as the first neglected term, $b_k Q_{k+1}(t)$, gives the back transfer to the included part of the chain from the neglected part, whereas transfer to the neglected part is already included in the diagonal term $-a_k Q_k(t)$. Thus, for any condition of the neglected part of the chain, straight truncation after a diagonal term results is a decay that is at least as fast as for any physical model consistent with the elements of $\mathbf{T}_k$. Applying this argument to adjacent levels of approximation shows that the right-hand side of eq 3.22 furnishes a sequence of nondecreasing lower bounds to $P(t)$ with increasing k: $P_{LB(1)}(t) \le P_{LB(2)}(t) \le ... \le P_{\mathrm{LB}(k)}(t)$.

In similar fashion, a non-increasing sequence of upper bounds is obtained by solving the eigenvalue problem associated with a sequence of modified matrices $\mathbf{T}_k^{UB}$. These differ from the matrices $\mathbf{T}_k$ only in assignment of the lower right element $(\mathbf{T}_k)_{kk}$

$$\mathbf{T}_k^{UB} = \begin{pmatrix} a_1 & b_1 & & & \\ b_1 & a_2 & \cdot & & \\ & \cdot & \cdot & & b_{k-1} \\ & & & b_{k-1} & c_k \end{pmatrix} \tag{3.24}$$

The new element, c_k, is determined by the condition that the determinant, $\det(\mathbf{T}_k^{UB})$ vanish. A little algebra shows that this condition is satisfied for c_k given by a continued fraction expansion in terms of previously generated elements

$$c_k = \cfrac{b_{k-1}^2}{a_{k-1} - \cfrac{b_{k-2}^2}{a_{k-2} - \cdot}} \qquad \cdot \qquad \cdot \qquad a_3 - \cfrac{b_2^2}{a_2 - \cfrac{b_1^2}{a_1}} \tag{3.25}$$

Note that in evaluating c_k the matrix element a_k is not required, and thus one less moment is required, for the determination of $\mathbf{T}_k^{UB}$.

Solution of the eigenvalue problem associate with $\mathbf{T}_k^{UB}$ yields a different set of k quadrature abscissas and weights, which in turn furnish a sequence of nonincreasing upper bounds to the left side of eq 3.17. These solutions are of the form

$$P_{UB(k)}(t) = \sum_{i=1}^{k} |\langle \mathbf{V}_i^{UB} | \psi(0) \rangle|^2 \exp(-\eta_i^{UB} t) \tag{3.26}$$

where the set $\{\eta_i^{UB}\}$ contains the eigenvalues and $\{\mathbf{V}_i^{UB}\}$ the corresponding eigenvectors of $\mathbf{T}_k^{UB}$. Equations 3.22 and 3.26 represented k-point quadrature approximations to the integral of eq 3.17 derived from the lower-order moments of $N_0(\lambda)$. Equations 3.24−3.26 for the upper bounds are equivalent to results obtained previously,[20] but can be derived more directly as follows: To rationalize that eq 3.26 indeed furnishes an upper bound of order k, imagine that the neglected part of the chain described by eqs 3.23 serves as a continuous source of occupation probability, feeding into the k^{th} transformed site. Any positive source will lead to a reduction of a_k. If the source is too strong, an unbounded (and unphysical) growth in occupation will occur at long time, as signified by the appearance of a negative eigenvalue when a_k is so reduced. Thus, there must be a maximal source, which reduces a_k to some new value c_k for which a zero eigenvalue first appears and the determinant of the modified matrix, $\det(\mathbf{T}_k^{UB})$, vanishes. This is precisely the condition that c_k equal the continued fraction of eq 3.25. Applying this argument to adjacent levels of approximation, as before, shows that the right-hand side of eq 3.26 furnishes a sequence of nonincreasing upper bounds to $P(t)$ with increasing k: $P_{UB(1)}(t) \geq P_{UB(2)}(t) \geq \ldots \geq P_{UB(k)}(t)$.

Coincident with the vanishing determinant, and the lowest eigenvalue of $\mathbf{T}_k^{UB}$ equaling zero, the upper bound solutions given by eq 3.26 approach constant values at long time. The asymptotic value for order k is determined by that eigenvector whose eigenvalue is zero. After some algebra we find

$$P_{UB(k)}(\infty) = \left\{1 + \left[\frac{\det(\mathbf{T}_1)}{b_1}\right]^2 + \left[\frac{\det(\mathbf{T}_2)}{b_1 b_2}\right]^2 + \ldots + \left[\frac{\det(\mathbf{T}_{k-1})}{b_1 b_2 \ldots b_{k-1}}\right]^2\right\}^{-1} \tag{3.27}$$

The sequence of positive terms in curly brackets serves to indicate the rate of convergence of the upper bounds to the exact decay.

The quadrature-based lower- and upper-bound approximations, given by eqs 3.22 and 2.26, respectively, generally converge much more rapidly than does a short-time moment series based on series expansion of the exponent within the integral of eq 3.17. Furthermore, the bounds are optimal as a physically valid model can always be constructed in which any specified upper or lower bound is realized. This is easiest seen by working with the transformed kinetic equations, eqs 3.23. The reason underlying improved convergence has been discussed previously in terms of linked-cluster expansions[19,20] and the arguments are easily transfer to the present situation. Specifically, contributions to $P(t)$ consist of Brownian-like loops in cluster size space that start at and return to the critical cluster size. (Clusters that never depart from critical size are of course also included.) Each unit step corresponds to either a monomer gain or a loss event. The recursion method includes to *infinite order* those loops which circulate repeatedly among clusters near critical size (i.e., clusters A_{g^*-m} through A_{g^*+m} for m levels of the algorithm and Krylov space dimensionality $m + 1$). The moment series expansion for $P(t)$, on the other hand, includes only those loop paths whose total length does not exceed $2m$. It is useful to generalize this concept using graph theory: Envisage the Brownian paths as graphs on a lattice containing the various cluster sizes as node points. In this language, the difference between the recursion method and the simple graphical expansion for the moments is equivalent to the difference between a linked cluster expansion, summing all lower-order paths to infinite order, and an approximation that simply generates all the lower-order graphs (paths) without resumming. Accordingly, the recursion method includes contributions to higher-order moments from paths that wind repeatedly throughout neighboring cluster sizes. For an initial cluster size of g^*, these are the very same paths that dominant the nucleation rate.

4. Fluctuations and Noise

The matrix-recursion method was developed in the previous section and used to track the continuous evolution of probability, $P(t)$, that a cluster initially of critical size is of critical size at time t. $P(t)$ describes an averaged relaxation process and is thus distinct from tracking the stochastic dynamics of individual clusters including fluctuations and noise. Fluctuations occur as the particle executes its Brownian-like walk in cluster size space as determined by the properties of the bath, the detailed balance condition, and the potential, $W(g)$, the gradient of which defines the field of force. This section takes the opposite approach by studing the statistics of the Brownian-like walks. The theory is based on the Kubo and Nyquist relations, which are demonstrated using a shot noise model to describe the exchange of molecules between cluster and bath.

Equation 2.5 has the form: *current = potential difference/resistance* with potential f_g/n_g, resistance $1/(\beta_g n_g)$, and current $J_{g,g+1}$. This resistor network "analogy", is often a convenient

way to think about nucleation currents, especially for binary and multicomponent nucleation where the networks have higher dimension.[23] However, the analogy is more of a mathematical guide and does not appear to have a direct physical significance. For example, a physical resistor will have associated with it Johnson noise through the Nyquist relation,[11] and the association of $1/(\beta_g n_g)$ with a resistance does not naturally yield such a relation. The origin of the difficulty lies in the fact that (f_g/n_g) is not a proper conjugate force in the sense of irreversible thermodynamics.[11] The problem is resolved by reformulating eq 2.5 in terms of the Nernst−Planck equation.[15] For this purpose, we take the continuum limit

$$J = -\beta n \nabla_g (f/n) \tag{4.1}$$

where the gradient is with respect to cluster size. This expression, together with equilibrium population of g-mers from eq 2.4, implies the Nernst−Planck equation

$$J_g = -\beta_g \nabla_g f - \beta_g \frac{f_g}{kT} \nabla_g W \tag{4.2}$$

The lead term on the right-hand side describes diffusion in cluster size space, with size-dependent diffusion constant $D = \beta_g$. The second term describes drift in the force field given by the gradient of W. (In cluster size space f and $\nabla_g f$ have the same units, cm^{-3}; D and β_g each have units of s^{-1}, and J_g has units of $cm^{-3}\ s^{-1}$.)

The nucleation barrier, together with any applied bias potential that might be added for non-Boltzmann sampling, constitutes the total potential, the gradient of which gives rise to (linear-response) drift of the cluster in size space with conductivity, per cluster, β_g/kT. Note that if the "equivalent" electrochemical potential is assumed to have the standard form, $\bar{\mu}(g) = \mu_0(T, P) + kT \ln f_g + W_g$, eq 4.2 becomes $J_g = -(\beta_g f/kT)(\partial\bar{\mu}/\partial g)_{T,P}$, which is the result demanded by irreversible thermodynamics.

Key quantities in eq 4.2, specifically the nucleation current, J, and the population gradient, $\nabla_g f$, cannot be easily determined from computer simulations of individual clusters. For example, the diffusion current, which is a statistical property of the full cluster distribution, cannot be determined this way. A more useful approach for studying single cluster motion in size space is to construct a Langevin equation[12] equivalent to eq 4.2

$$\dot{g} = -\frac{\beta_g}{kT} \nabla_g W + J_r(t) \tag{4.3}$$

Here $\dot{g} = dg/dt$ is the single particle current (equal to the change in the number of molecules in the cluster with time), and β_g/kT is the single-particle mobility consistent with the Nernst relation ($D = kT \times$ *mobility*). $J_r(t)$ is the fluctuating current in the field-free reference system ($\nabla W = 0$)—realizable through the application of a bias potential chosen to locally cancel the nucleation barrier (unbiased) gradient. The lead term on the right of eq 4.3 gives the drift motion due to the gradient force, and the inverse mobility, $R = kT/\beta$, is the resistance to this force. We now show that this definition of the resistance *is* compatible with the Nyquist relation and identify the associated noise.

Any analysis must first include a criterion for determining which sets of molecules form a cluster. The Stillinger criterion,[27] in which a molecule is counted as part of the cluster if it is within some specified distance from another molecule in the cluster is a good example, although other criteria can be used.[28,29] In any of these models, changes cluster size take place instantaneously as single molecules or groups of molecules cross the criterion boundary. Although the gain and loss of monomer generally dominates the kinetics, the importance of multimolecule additions and subtractions has been demonstrated—as has the validity of detailed balance for such multimolecular steps.[3] However, the multimolecular transitions were found to be mainly due to the arrival and departure of smaller clusters.[3] Presumably, if these clusters were absent from the parent phase the multimolecular steps would be correspondingly reduced. Here, we will assume that the parent phase is dominated by monomer and higher-order transitions are neglected.

Under these conditions, the fluctuation current in eq 4.3 is a series of uniform delta functions as depicted in Figure 3. The figure shows a sequence of evaporation/growth events obtained from a single realization of the stochastic model described here and in section 5. Additionally, it is assumed that molecular addition and loss are statistically independent,[30] which is consistent for thermalization on a time short compared with the collision time. Under these conditions, the fluctuating current separates into its forward (condensation) and reverse (evaporation) components: $J_r = J_r^+ - J_r^-$ with $J_r^+ = \sum\delta(t - t_i)$ where the t_i's are the random times of molecular addition events, and similarly for J_r^-. The delta function currents may be expanded into their (white noise) frequency components as described in Lawson and Uhlenbech.[31] After applying a similar expansion for the reverse currents (cross terms vanish from the assumption of statistical independence), the following result for the spectral density of fluctuations in the current J_r at frequency ν_k is obtained

$$G_{Jr}(\nu_k) = 4\beta = 4kT/R \tag{4.4}$$

For notational simplicity the subscript "g" has been omitted.

The single-particle mobility β/kT is related to the autocorrelation of the random current through the Kubo formula[11,13−15]

$$\frac{\beta}{kT} = \frac{1}{kT}\int_0^\infty \exp(-2\pi\nu_k t)\langle J_r(0), J_r(t)\rangle dt = \frac{1}{4kT} G_{Jr}(\nu_k) \tag{4.5}$$

The frequency independence of the left-hand side, which is consistent with $J_r(t)$ having the properties of white noise, is a characteristic of the shot noise model. From eq 4.4 and the last equality of eq 4.5, we obtain the Nyquist relation[11,31]

$$G_{J_r}(\nu_k)\Delta\nu = \langle J_r^2\rangle_{\Delta\nu} = \frac{4kT}{R}\Delta\nu \tag{4.6}$$

The middle expression gives the power spectrum of the current fluctuations as measured through a filter having frequency bandwidth $\Delta\nu$. These arguments show that the proper "physical" resistance, given by $R = kT/\beta$, is indeed associated with classical thermal noise (i.e., quantum effects are not evident). The thermal noise, in turn, derives from fluctuations inherent in the (shot-like) exchange of molecules between cluster and bath and is fundamentally connected with the resistance through the Nyquist relation.

5. Calculations and a Duality Model

This section describes calculations based on the shot noise properties of the molecular exchange between a cluster and its surroundings. The present cluster model does not have any molecular detail, but is instead based on classical nucleation theory, for which the cluster free energy is given by eq 2.10. The resulting stochastic model is in fact very similar to the one developed in ref 30. The essential difference is that here it is

assumed that clusters are rapidly thermalized with respect to their surroundings, i.e., thermalized on a time scale short compared to the average time (of order $1/\beta_{g^*}$) of molecular exchange.

The model is defined as follows: Evaporation and growth events are treated as independent, Poisson-distributed processes. The growth sequence is simulated using Poisson arrival times for monomer at a fixed mean rate $\beta_g = (g/g^*)^{2/3}\beta_{g^*}$ based on the scaling of the cluster surface to volume implicit in the classical theory. As in eq 2.9, the g dependence here is found to have very little effect on the dynamics of barrier crossing. This dependence is retained here for the barrier simulations, and neglected for the duality model, described below, for which the extra symmetry gained by having a size-independent β is required. The evaporation sequence is also simulated using Poisson statistics with mean rate determined from β_g and $W(g)$ using detailed balance (eq 2.4). The computational time step (τ) is set sufficiently small that the occurrence of multiple events, within a single time step, is rare. Model runs were previously found to be independent of this setting for values of τ below about 1/10 of the average collision time.[30] For the present simulations $\tau = 0.025/\beta_{g^*}$.

With time expressed in units of $1/\beta_{g^*}$, many of the results about to be presented would be substance independent—as the only model parameters left are g^* and W* (cf. eq 2.10). For specificity, the methods are demonstrated below for homogeneous nucleation of water vapor at $T = 300$ K and at a saturation ratio chosen so that $g^* = 100$. Classical nucleation theory, together with the known properties of water, predicts that this condition occurs for a critical saturation ratio of about 3.2 and yields a barrier height W^* of about 57.9 kT and mean collision time $1/\beta_{g^*} \cong 2.47 \times 10^{-10}$ s.

Figure 3 shows a sample sequence of cluster growth and evaporation events obtained from a single, short-time run of the model as described in section 4. These events illustrate shot behavior, but the sampling is insufficient for garnering any meaningful statistical information on the parameters that determine nucleation rate. Figure 4 shows cluster size as a function of time—again for a single trajectory realization of the model. The initial condition is $g = g^* = 100$. The figure reveals essentially random excursions about the top of the barrier, with multiple recrossings, followed some time later by sustained growth. Once well into the growth regime, the probability of another recrossing is negligibly small.

Figure 5 (noisy solid curve) shows the relaxation function $P(t) = \langle g^*|\psi(t)\rangle$ estimated by averaging 1000 trajectories, each obtained in the manner of Figure 4. The value at time t is determined as follows: For each run examine the cluster size at time t; if this happens to be g^*, assign a value of 1, otherwise 0. Finally, sum the results from each run and divide by 1000. The figure also shows the first, third, and tenth upper and lower bound pairs on $P(t)$ from the matrix-recursion method. The first upper bound corresponds to no decay, $P_{\mathrm{UB}(1)}(t) = 1$. The tenth upper and lower bound pairs are converged on the scale of the figure, and remain converged for about the first 10 ns. Note that although the simulation goes outside of the bounds, this is allowed because the matrix-recursion method yields bounds to the decay probability while the simulated decay, even after averaging 1000 runs, is still only a sampling and not a true probability.

The nucleation rate is related to the area under $P(t)$. To show this, let r denote the fraction of critical clusters that ultimately escape to the growth regime (typically $r \cong {}^1/_2$). Then $1 - r$ is the fraction that ultimately evaporate. Flux balance considerations imply for the steady-state nucleation current

$$J = r f_{g^*} / \int_0^\infty P(t)dt \tag{5.1}$$

For $P(t)$ equal to the pure exponential decay of the first lower-bound, $P_{LB(1)}(t)$, the right side of eq 5.1 reduces to the rate predicted by transition state theory. From section 2, this is an upper bound on the true rate. Improved upper bounds on J result upon substitution of higher-order *lower bounds* on $P(t)$ into eq 5.1 and, because these are nested, the value of the denominator always increases, and the upper bound on J always decreases, with increasing k. Figure 5 highlights the difficulty of inferring a nucleation rate from simulations of individual cluster dynamics. Specifically, it is difficult to evaluate the integral using just the converged part of the decay. For example, from the converged 10th pair of bounds one cannot, on this time scale, get even a reliable estimate for the *sign* of the curvature of $W(g)$. Indeed the converged bounds are fit very well over the range of Figure 5 by the function

$$\mathrm{d}(t) \equiv (4\pi D t)^{-1/2} = (4\pi\beta_{g^*} t)^{-1/2} \tag{5.2}$$

where the right side may be recognized as the expected decay due to diffusion alone[32] when the potential is flat! On the other hand it is not useful for this problem to increase the order of recursion. The advantages of recursion (and related projection operator methods generally) are greatest when the subspace dimension can be made small, not to mention the ill-conditioning associated with working with higher-order moments.

A potentially useful approach is suggested by a recent study of nonequilibrium dynamics in one-dimensional random environments.[16] Using real space renormalization group methods, these authors studied diffusion on a one-dimensional potential landscape, itself random, and describe a duality equivalent to reversing the sign of the average force. In the present context, force reversal is achieved simply by inverting the nucleation barrier to get a mirror-symmetric potential well. Barrier and dual well surfaces are shown in Figure 6 for the present example ($g^* = 100$, $W^* = 57.9kT$).

From eq 2.4, the equilibrium distribution for clusters in the well, n'_g, is inversely related to the constrained equilibrium distribution for the barrier

$$\frac{n_{g^*}}{n_g} = \frac{n'_g}{n'_{g^*}} \tag{5.3}$$

Introducing the additional symmetry gained by setting $\beta_g \cong \beta_{g^*}$, allows one to rewrite eq 2.9 for the barrier transmission coefficient

$$\kappa \cong \left(\sum_g \frac{n_{g^*}}{n_g}\right)^{-1} = \left(\sum_g \frac{n'_g}{n'_{g^*}}\right)^{-1} = \frac{n'_{g^*}}{\sum_g n'_g} = P_{\mathrm{WELL}}(\infty) \tag{5.4}$$

where $P_{\mathrm{WELL}}(t)$ is the relaxation function for the well (analogous to $P(t)$ for the barrier) and $P_{\mathrm{WELL}}(\infty)$ its value in the limit that equilibrium has been reached. Figure 7 shows a sample trajectory for the well. This differs from the barrier case (Figure 4) in that the fluctuations are contained by the well potential and a cluster never, with any reasonable probability, undergoes either complete evaporation or significant growth. As a potential for non-Boltzmann sampling, the dual well has the optimal property that it gives cluster weights in proportion to their contribution to the nucleation rate. Figure 8 shows a statistical

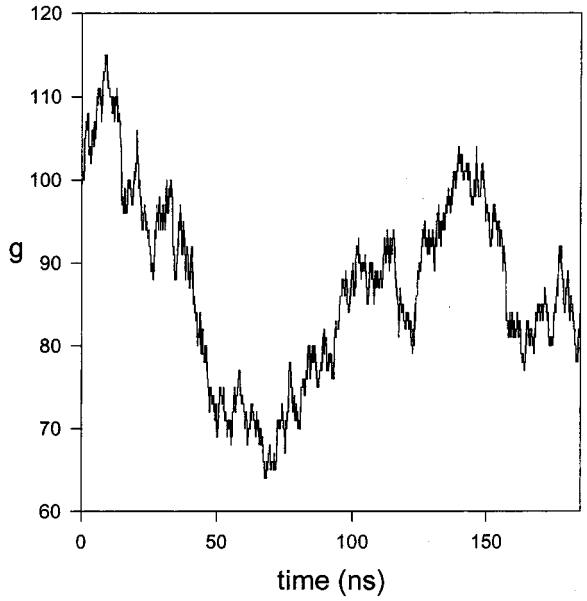

Figure 7. Cluster size as a function of time for a simulated trajectory in the dual well of Figure 6.

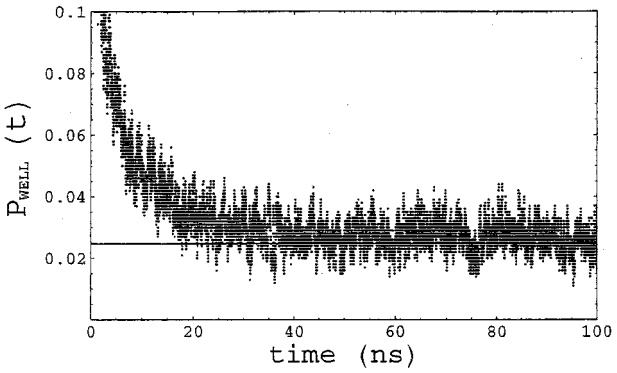

Figure 8. Simulated decay, $P_{\mathrm{WELL}}(t)$, obtained from the stochastic model for the dual well potential of Figure 6. The result shown was obtained by averaging 1000 trajectories as described in the text. Good agreement results when the asymptotic (equilibrium) decay state for the well is compared with the transmission coefficient ($\kappa = 0.248$) for the corresponding barrier (horizontal line).

sampling of $P_{\mathrm{WELL}}(t)$ obtained by an averaging of 1000 runs. The calculation is similar to the one used to obtain the noisy curve of Figure 5, except that here the potential has been inverted and the simulation carried out to significantly longer time. The asymptotic decay to the well equilibrium state approaches, as expected from eq 5.4, the barrier transmission coefficient, which for the present conditions has the value $\kappa = 0.248$ indicated by the horizontal line. This last result shows that, albeit with extensive sampling, the barrier transmission coefficient can be estimated using non-Boltzmann trajectories evolving in the dual potential of the inverted well.

The limit that the barrier is flat (zero drift), corresponds to criticality in the duality model and is approached as g^* becomes large. Here for $g^* = 100$ simulation difficulties associated with criticality have already emerged: transport coefficients such as κ are small, a large number of clusters contribute essentially equally to the dynamics, and one has difficulty even determining the sign of the curvature from simulations on the molecular scale. For larger values of g^*, where one is even closer to criticality, different methods—perhaps based on first transforming the system away from criticality using decimation and real space renormalization methods similar to those of ref 16—will need to be developed. While these considerations are beyond the scope of the present study, a few additional properties of the duality model are worth noting.

Equation 5.4 has usual form of a fluctuation−dissipation theorem in that a transport parameter, κ, is related to an equilibrium property, here the equilibrium cluster distribution, but with respect to the dual potential, and not the original one for which a true equilibrium state does not exist. Other connections between the steady-state nucleation rate for a given barrier and the equilibrium state for the dual well can be listed. For example, as nucleation approaches steady state, the function ϕ_g defined below (see also section 2)

$$\phi_g \equiv \frac{f_g}{n_g} - \frac{f_{g+1}}{n_{g+1}} \rightarrow \frac{1/n_g}{\sum_i 1/n_i} = \frac{n'_g}{\sum_i n'_i} = \frac{f'_g(\infty)}{\sum_i f'_i(\infty)} = f'_g(\infty) \qquad (5.5)$$

approaches the equilibrium probability for distribution of a cluster in the well. The latter distribution maximizes entropy at equilibrium while the former minimizes the rate of entropy production at steady state. The focus on the dynamics of single clusters results in the dual normalization conditions: $\sum\phi_g = \sum f'_g = 1$, which are preserved over time. The first is simply a consequence of the monomer and Szilard boundary conditions of section 2, and the second is normalization to a single cluster. At criticality, the dynamics has pure diffusive character and it is readily shown from the matrix equations of section 3 that $\phi_g(t)$ and $f'_g(t)$ have identical dynamical behavior for all time beginning with the initial conditions: $\phi_{g^*}(0) = f'_{g^*}(0) = 1$.

6. Summary

This paper has examined the dynamics of nucleation barrier crossing using a shot-noise model for fluctuations in cluster size and classical nucleation theory for the cluster free-energy. The matrix-recursion method has been developed as a new tool for describing the average relaxation from the top of the free-energy barrier, and yielding nested pairs of upper and lower bounds to the relaxation rate. Results from sections 2−5 demonstrate the difficulties associated with estimating either the barrier transmission coefficient or nucleation rate from simulation of single-cluster size change events. The duality model provides at least a qualitative explanation by suggesting that these difficulties, which arise mainly form the large numbers of clusters contributing nearly equally to the dynamics, are indicative of a near-criticality condition. From this perspective, it is not surprising that it is exceedingly difficult to abstract global nucleation rates from the single-molecule kinetics of individual clusters undergoing evaporation and growth. What is needed is a way to eliminate the fast, essentially irrelevant, dynamics while accurately retaining information on the long-time behavior governing the overall nucleation process. For systems that have inherent time scale separation, perhaps the best example being the binary, vapor phase, nucleation of sulfuric acid and water, a very effective—even quantitative—method is available.[34] However, for systems without inherent time scale separation, new approaches to the kinetics, perhaps based on renormalization group methods,[16] will be required. These are topics for future research.

It should be noted that all of the results obtained in this paper apply equally well to a generalization of the CNT based on the Kelvin relation.[33] That theory develops the idea that if the Kelvin relation is satisfied, the barrier can differ from eq 2.10 only by a uniform displacement in energy: $W(g) = W_{CNT}(g) + D(T)$

where $D(T)$ is a function of temperature alone. Consequently, κ is identical in the CNT and Kelvin-based models. Indeed, the only difference is that the two models will generally have different transition state theory rates, J_{TST}, due to the shift in barrier height.

Although the present development treats clusters within the capillarity drop approximation, it is reasonable to expect many of the essential features of barrier crossing derived from this model to carry over qualitatively, if not quantitatively, to molecular simulations. This expectation is supported by recent simulations of nucleation in a Lennard−Jones system,[1,2] which found good agreement with CNT for overall barrier shape—a displace CNT barrier in support of the Kelvin model,[1] and small barrier transmission coefficient[2] consistent with the values shown in Figure 1. Nevertheless, the Bennett-Chandler and Kramers models have traditionally been applied to molecular systems. The application of transition state methods to nucleation, for which the primary coordinate is cluster size and the transition state corresponds to a single critical cluster size, remains an active area of research[1,2,4,35]

Acknowledgment. The author wishes to thank Profs. Howard Reiss and Pierre Schaaf, and Dr. Richard Bowles for many productive discussions during a week at UCLA hosted by Prof. Reiss. This research was supported in part by NASA as part of its interdisciplinary research program on tropospheric aerosols and in part by the Environmental Sciences Division of DOE.

References and Notes

(1) ten Wolde, P. R.; Frenkel, D. *J. Chem. Phys.* **1998**, *109*, 9901.
(2) ten Wolde, P. R.; Ruiz-Montero, M. J.; Frenkel, D. *J. Chem. Phys.* **1999**, *110*, 1591.
(3) Schaaf, P.; Senger, B.; Voegel, J.-C.; Bowles, R.; Reiss, H. *J. Chem. Phys.* **2001**, *114*, 8091.
(4) Kathmann, S. M.; Schenter, G. K.; Garrett, B. C. *Aerosol Science and Technology Series* **2000** (Frontier-Science Research Conference, La Jolla International School of Science, Institute for Advanced Physics Studies, April 24).
(5) Reiss, H.; Kegel, W. K.; Katz, J. L. *J. Phys. Chem. A* **1998**, *102*, 8548.
(6) Berg, B. A. *Nucl. Phys. Proc. Suppl.* **1998**, *63*, 982.
(7) Ruiz-Montero, M. J.; Frenkel, D.; Brey, J. J. *Molecular Physics* **1997**, *90*, 925.
(8) Kramers, H. A. *Physica* **1940**, *7*, 284.
(9) Reguera, D.; Rubi, J. M.; Perez-Madrid, A. *J. Chem. Phys.* **1998**, *109*, 5987.
(10) Shugard, W. J.; Reiss, H. *J. Chem. Phys.* **1976**, *65*, 2827.
(11) Wannier, G. H. *Statistical Physics*; Dover: New York, 1966.
(12) Kubo, R. In *Tokyo Summer Lectures in Theoretical Physics, Part I: Many Body Theory*; Benjamin: New York, 1965; pp 1−16.
(13) Bashkirov, A. G.; Fisenko, S. G. *Teoreticheskaya i Mathematicheskaya Fizika* **1981**, *48*, 106.
(14) Reguera, D.; Rubi, J. M.; Perez-Madrid, A. *Physica A* **1998**, *259*, 10.
(15) McGraw, R.; Schaaf, P.; Reiss, H. In *Nucleation and Atmospheric Aerosols 2000 15th International Conference Rolla, Missouri 2000*, AIP Conference Proceedings; Hale, B. N., Kulmala, M.; Eds.; AIP: New York, 2000; Vol. 534, pg 3.
(16) Fisher, D. S.; Le Doussal, P.; Monthus, C. *Phys. Rev. Lett.* **1998**, *80*, 3539.
(17) Abraham, F. F. *Homogeneous Nucleation Theory*; Academic: New York. 1974.
(18) Onasch, T. B.; McGraw, R.; Imre, D. *J. Phys. Chem.* **2000**, *104*, 10 797.
(19) Haydock, R.; Heine, V.; Kelly, M. J. *J. Physics C.* **1975**, *8*, 2591; **1972**, *5*, 2825.
(20) McGraw, R.; Merry, G. A. *Chem. Phys.* **1985**, *96*, 97.
(21) McGraw, R. *Aerosol Sci. and Technol.* **1997**, *27*, 255.
(22) Wright, D. L.; McGraw, R.; Benkovitz, C. M.; Schwartz, S. E. *Geophys. Res. Lett.* **2000**, *27*, 967.
(23) McGraw, R. *J. Chem. Phys.* **1995**, *102*, 2098.
(24) Gordon, R. G. *J. Math. Phys.* **1968**, *9*, 655.
(25) Mori, H. *Prog. Theor. Phys.* **1965**, *34*, 399.
(26) Press, W. H.; Teukolsky, S. A.; Vetterling, W. T.; Flannery, B. P. *Numerical Recipes in FORTRAN*; Cambridge University Press: Cambridge. 1992.
(27) Stillinger, F. H. *J. Chem. Phys.* **1963**, *38*, 1486.
(28) Senger, B.; Schaaf, P.; Corti, D. S.; Bowles, R.; Voegel, J.-C.; Reiss, H. *J. Chem. Phys.* **1999**, *110*, 6421.
(29) Senger, B.; Schaaf, P.; Corti, D. S.; Bowles, R.; Pointu, D.; Voegel, J.-C.; Reiss, H. *J. Chem. Phys.* **1999**, *110*, 6438.
(30) McGraw, R.; LaViolette, R. A. *J. Chem. Phys.* **1995**, *102*, 8983.
(31) Lawson, J. L.; Uhlenbech, G. E. *Threshold Signals*; Dover: 1950; p 79.
(32) Chandrasekhar, S. In *Selected Papers on Noise and Stochastic Processes*; Wax, N., Ed.; Dover: New York, 1954.
(33) McGraw, R.; Laaksonen, A. *J. Chem. Phys.* **1997**, *106*, 5284.
(34) Shugard, W. J.; Heist, R. H.; Reiss, H. *J. Chem. Phys.* **1974**, *61*, 5298.
(35) Kathmann, S. M.; Schenter, G. K.; Garrett, B. C. *J. Chem. Phys.* **1999**, *111*, 4688.